3 State Current Mode of a Grid Connected PV Converter

Attila Balogh, Eszter Varga, and István Varjasi

Abstract—Nowadays in applications of renewable energy sources it is important to develop powerful and energy-saving photovoltaic converters and to keep the prescriptions of the standards. In grid connected PV converters the obvious solution to increase the efficiency is to reduce the switching losses. Our new developed control method reduces the switching losses and keeps the limitations of the harmonic distortion standards. The base idea of the method is the utilization of 3-state control causing discontinuous current mode at low input power. In the following sections the control theory, the realizations and the simulation results are presented.

Keywords—Discontinuous current, high efficiency, PV converter, control method.

I. INTRODUCTION

THE photovoltaic arrays are pretty expensive, so it is needed to use them with the highest efficiency. The most frequent main circuit arrangement is the three phase bridge. The main advantage of our method is, that it is unnecessary to change the aforementioned topology of the converter, only the modification of the control is needed. In our previous work we successfully developed and used this control method in single phase photovoltaic converters [1]. In this paper we will introduce an algorithm developed for three phase converters. The presented method joins the benefits of Flat-top modulation – used in continuous mode control for decreasing switching losses – with the discontinuous mode control developed earlier for single phase converters.

Manuscript received March 26, 2008

Attila Balogh is with the Budapest University of Technology and Economics, Department of Automation and Applied Informatics, Budapest, Hungary (phone: +36 (1) 463 1552, fax: +36 (1) 463 2871, e-mail: balogh@aut.bme.hu).

Eszter Varga is with the Budapest University of Technology and Economics, Department of Automation and Applied Informatics, Budapest, Hungary (phone: +36 (1) 463 1552, fax: +36 (1) 463 2871, e-mail: hukk01@gmail.com).

Istvan Varjasi, PhD, is with the Budapest University of Technology and Economics, Department of Automation and Applied Informatics, Budapest, Hungary (phone: +36 (1) 463 1552, fax: +36 (1) 463 2871, e-mail: varjasi@aut.bme.hu).

II. THE TOPOLOGY OF OUR CONVERTER

The main parts of the converter are: the PV array, the Boost DC/DC converter and the three phase inverter with filters (see Fig. 1). The PV array converts the solar energy to DC power. An optional step-up converter may raise the voltage level of the PV array to the voltage level of the three phase bridge.
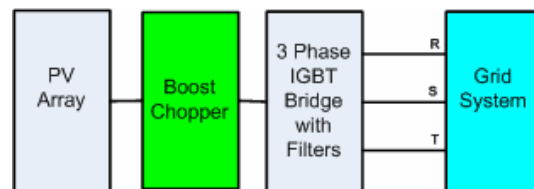

Fig. 1 Topology of the converter

The control of the boost chopper algorithm includes the maximal power point tracking (MPPT). The boost chopper is not necessary when the voltage of the array at MPP is greater than the peak line voltage of the grid. In that case the reference of the dc voltage is derived from the MPPT algorithm. The three-phase bridge converts the dc voltage to nearly sinusoidal ac currents. The high order harmonics of the output current are filtered out by passive low-pass filter.

III. THE TRADITIONAL CONTROL

There are several control methods of the grid connected PV converter. Most of them consist of an outer control loop for the DC voltage and inner current control loop. From these we use the grid voltage oriented current control. This control structure is very similar to the field oriented control (FOC) of ac machines. The controllers work here also in a rotating frame, but this rotating frame is connected to the grid voltage vector, so we may named this control system as grid voltage oriented control. The current component in the direction of the grid voltage vector is named as current "d" and is proportional to active power, while the orthogonal current component is named as current "q" and is proportional to reactive power. In this arrangement there is no zero order current, so it is enough to measure only two currents. The phase currents are transformed to the rotating d-q coordinate-system [2]. For the current control the currents are sampled at symmetry point(s) of PWM cycle, so the sampled current is close to the average value for a given switching period.

IV. THE SUGGESTED CONTROL METHOD

The developed inverter control has to satisfy two groups of requirements. On one hand the dc source energy should be feed-back to the ac network with an efficiency as high as possible. On the other hand the prescriptions of the standards must be full-filled for the utility compatibility. According to the standards, the ac currents should be nearly sinusoidal, and the power factor should be greater than 0.95. By reduction of the switching losses with the proposed method we may increases the efficiency while maintaining the limitations of standards.
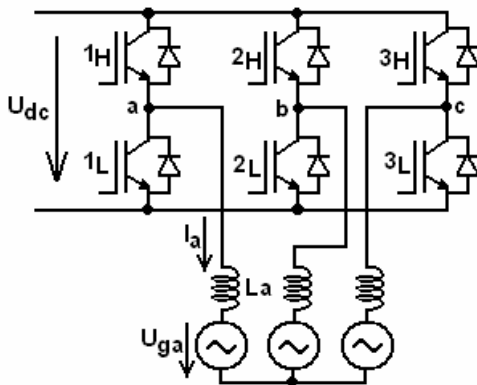

Fig. 2 The main circuit

In case of PV converters the efficiency can be calculated as the weighted average of efficiencies measured at the 10%, 50% and 90% of nominal power [3]. With the traditional control it is very hard to reach a good efficiency at 10% of nominal load, since the iron losses of filter choke will the same, and the switching-off losses of the IGBT-s will be comparable to the losses at nominal load. Our method above all with the increasing of the efficiency at 10% load would reach a better weighted efficiency.

The new control algorithm reaches better efficiency utilizing the discontinuous current mode (see abstract). The IGBT-s in the direction of the reference current will be switched (see lower curve at Fig. 3). With this control the switching-on losses of the IGBT would be zero, the iron losses and the switching-off losses would be smaller [4]-[9].

Unlike with traditional control, there is no symmetry point of the switching period, so the sampled current will not be equal to the average current. In the following we will introduce a method how this relationship can be calculated in continuous and discontinuous current mode.

While the idea seems quite simple, the method is very complicated, since the current of the three phases aren't independent, and the discontinuous phase reacts on the voltage of the other phases.

When developing the algorithm we prescribed some simplification and limitation. These are the followings:

- the converter doesn't make reactive power,
- in the phase where the absolute value of the current reference is the highest, one IGBT is turned on for the whole switching period,
- at least in two inductors the currents are continuous for one switching period,
- $U_{ga}+U_{gb}+U_{gc}=0$, symmetrical grid voltage,
- there isn't common mode current.

These limitations are true for the most grid connected PV converters.

Let's investigate at the moment, when the line voltage between a and c phases reaches its positive maximum. IGBT 1H and 3L will have near 100% duty cycle (see Fig. 2).

The following conditions are valid at the investigated moment:

- $Ua > Ub > Uc < 0$, $Ub < 0$.

Considering similar conditions there are 12 control sections. In this paper only the first control section's equations are obtained, the other 11 states can be calculated from these, with rotating the voltage vectors.

With the traditional control IGBT 2H and 2L of the middle leg with near 50% duty cycle make the voltage of the phase *b*. The current of the phase *b* with a small average value cyclic changes between positive and negative values (see upper curve at Fig. 3). The cyclic change would result significant switching and iron losses.
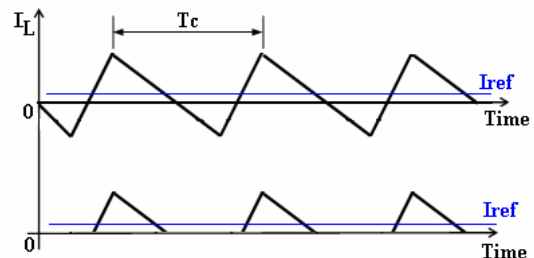

Fig. 3 Current waveforms

In this section the mathematical description of the continuous algorithm is presented. The continuous current mode waveforms can be seen in Fig. 4.

A. Continuous Operational Mode

In continuous current mode there are three different switching states (see Fig. 4), in the first one 1H,2H,3H IGBT-s, in the second one 1H,2H,3L while in the third one 1H,2L,3L are turned on.
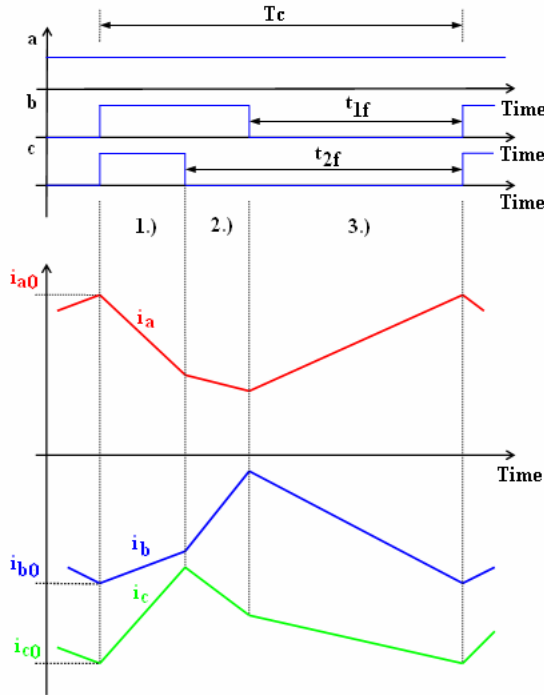
Fig. 4 Continuous waveforms

In the first step the change of rate of inductor currents is calculated in the three switching states.

The change of rate of inductors current in the first switching state in phase b and c is the following:

$$\frac{di_{b1}}{dt} = -\frac{u_{gb}}{L}, \frac{di_{c1}}{dt} = -\frac{u_{gc}}{L} \quad , \quad (1)$$

where U_{gb} and U_{gc} are the grid voltages and L is the grid side inductor of the converter.

In the second switching state the rates are:

$$\frac{di_{b2}}{dt} = \frac{-u_{gb} + \frac{1}{3}u_{dc}}{L}, \frac{di_{c2}}{dt} = \frac{-u_{gc} - \frac{2}{3}u_{dc}}{L} \quad . \quad (2)$$

While in the third one:

$$\frac{di_{b3}}{dt} = \frac{-u_{gb} - \frac{1}{3}u_{dc}}{L}, \frac{di_{c3}}{dt} = \frac{-u_{gc} - \frac{1}{3}u_{dc}}{L} \quad . \quad (3)$$

For repetitive current waveform t_{1f} and t_{2f} switching times can be approximated as:

$$t_{1f} = \frac{U_{ga} - U_{gb}}{U_{dc}} T_c \quad (4)$$

where Tc is the PWM cycle time.

$$t_{2f} = \frac{U_{ga} - U_{gc}}{U_{dc}} T_c \quad (5)$$

For the current control we need the relationship between the average value and the sampled value of the inductors currents. The current in phase b at the end of switching states can be calculated from (1)(2)(3) and (4)(5) as follows:

$$i_{b1} = i_{b0} + \frac{di_{b1}}{dt}(T_c - t_{2f}) \quad . \quad (6)$$

$$i_{b2} = i_{b1} + \frac{di_{b2}}{dt}(t_{2f} - t_{1f}) \quad . \quad (7)$$

$$i_{b3} = i_{b2} + \frac{di_{b3}}{dt}t_{1f} \quad , \quad (8)$$

where i_{b1} is the phase b current at the end of the first switching state, i_{b2} is at the end of second switching state, while i_{b3} is at the end of the PWM cycle time.

In steady state the current at the start and at the end of the PWM cycle time should be equal ($i_{b3} \approx i_{b0}$), so the sum of the current changes is zero:

$$\frac{di_{b1}}{dt}(T_c - t_{2f}) + \frac{di_{b2}}{dt}(t_{2f} - t_{1f}) + \frac{di_{b3}}{dt}t_{1f} = 0 \quad . \quad (9)$$

From (6)(7)(8) and (9) the average value of the phase b current can be calculated as follows:

$$i_{bAV} = \frac{1}{T_c}\left(\frac{i_{b0} + i_{b1}}{2}(T_c - t_{2f}) + A\right) \quad , \text{where}$$

$$A = \frac{i_{b1} + i_{b2}}{2}(t_{2f} - t_{1f}) + \frac{i_{b2} + i_{b3}}{2}t_{1f} \quad . \quad (10)$$

Substituting (4)(5) in (10) the average value of the current is:

$$i_{bAV} = i_{b0} - \frac{T_c}{6LU_{dc}}\left(3U_{gb}U_{dc} + B\right) \quad , \text{where}$$

$$B = 7U_{gb}^2 + 4U_{gb}U_{gc} - 2U_{gc}^2 \quad . \quad (11)$$

The average value of phase c current can be calculated similarly to the phase b. Without demonstration the average value of phase c is:

$$i_{cAV} = i_{c0} - \frac{T_c}{6LU_{dc}}\left(3U_{gc}U_{dc} + C\right) \quad , \text{where}$$

$$C = 7U_{gc}^2 + 4U_{gb}U_{gc} - 2U_{gb}^2 \quad . \quad (12)$$

Equation (11) and (12) establishes connection between the sampled current (i_{b0} and i_{c0}) and the average current.

B. Discontinuous Operational Mode

In this section the discontinuous current mode are presented. In the first step the continuous-discontinuous current limit should be calculated.

At small load the current of the phase b become discontinuous. For calculating the continuous-discontinuous current limit the maximal current of the phase b should be calculated.

The maximal current in phase b can be calculated from (8). Solving the equations:

$$i_{b\max} = i_{b0} + t_{1f} \frac{U_{gb} + \frac{1}{3}U_{dc}}{L}.$$ (13)

If i_{bmax} is greater than zero (see Fig.4.) discontinuous current mode is occurred, because in continuous current mode the i_b current is always negative.

In discontinuous current mode there are three different current modes depending on the load. These are *Disc1*, *Disc2* and *Disc3* operational modes.

In the next subsections the three operational modes, the current waveforms of phase c and the main equations are presented.
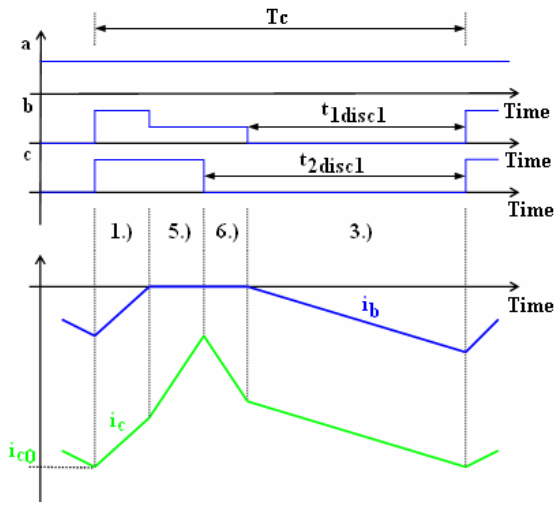
1.) Disc1 operational mode

Fig. 5 Disc1 mode waveform

In Fig. 5 the current of the phase c and the switching times can be seen. In phases a and c the current is always continuous, while in phase b during the section 5 and 6 the current is zero.

The current in phase b reaches zero before switching on 3L and $t_2 > t_1$.

The change of rate of the inductor current in phase c during section 5:

$$\frac{di_{c5}}{dt} = \frac{u_{ga} - u_{gc}}{2L},$$ (14)

while during the section 6 is:

$$\frac{di_{c6}}{dt} = \frac{u_{ga} - u_{gc} - u_{dc}}{2L}.$$ (15)
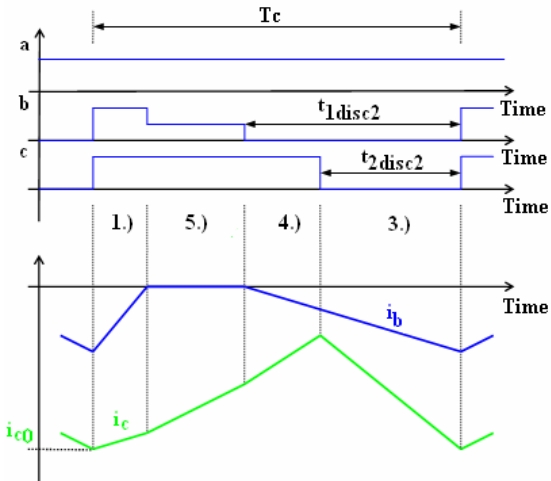
2.) Disc2 operational mode ($t_1 > t_2$)

Fig. 6 Disc2 mode waveform

In Fig. 6 also the current of the phase c and the switching times can be seen. In phases a and c the current is also always continuous, while in phase b during the section 5 it is zero.

The change of rate of the inductors current in phase b and c during the section 4 are:

$$\frac{di_{b4}}{dt} = -\frac{u_{gb} + \frac{2}{3}u_{dc}}{L}$$ (16)

$$\frac{di_{c4}}{dt} = \frac{-u_{gc} + \frac{1}{3}u_{dc}}{L}.$$ (17)

3.) Disc3 mode

The current in phase b reaches zero after 3L is switched on, $t_2 > t_1$.
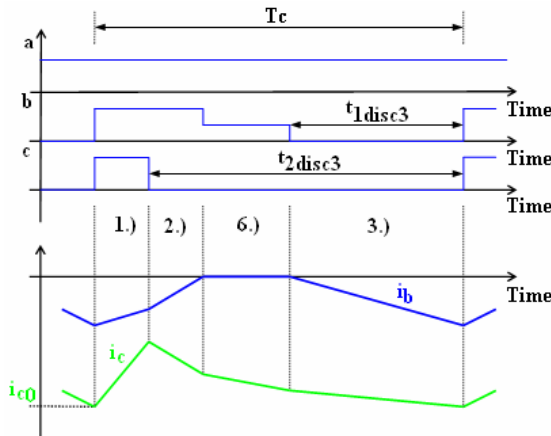

Fig. 7 Disc3 mode waveforms

In Fig. 7 the current of the phase c and the switching times can be seen. In phases a and c the current is also always

continuous, while in phase *b* during the section 6 it is zero. Accordance with the simulations this operational mode is the most frequent one.

The operational mode depends on the load of the phase *b* and on the Disc1-2 limit current.

The Disc1-2 limit current can be calculated as follows:

$$i_{bdisc12} = T_c \frac{(3U_{gb} + U_{dc})(U_{gc} + 2U_{gb})}{3LU_{dc}} \quad . \tag{18}$$

Equation (18) is true for moment values, since the algorithm uses average values, the average Disc1-2 limit current should be calculated.

Without demonstration the average value is the following:

$$i_{bdisc12AV} = \frac{1}{T_c}\left(\frac{t_{2disc12}^2}{2}\frac{di_{b3}}{dt} + D\right) \text{, where}$$

$$D = \frac{di_{b1}}{dt}\left(-\frac{t_{2disc12}}{2}\frac{di_{b3}}{di_{b1}}\right) . \tag{19}$$

In steady state the start and end value of the current in the PWM cycle is equal. With this condition solved, the limit current is:

$$i_{bdisc12} = -\frac{T_c}{18LU_{gb}U_{dc}^2}\left(18U_{gb}^4 + E\right) \text{, where}$$

$$E = 72U_{gb}^3U_{gc} + 72U_{gc}^2U_{gb}^2 + 9U_{dc}U_{gb}^3 + F$$

$$F = 36U_{dc}U_{gc}U_{gb}^2 + 36U_{gc}^2U_{dc}U_{gb} + G$$

$$G = U_{dc}^2(U_{gb}^2 + 4U_{gc}U_{gb} + 4U_{gc}^2) . \tag{20}$$

If $i_{bavref} < i_{bdisc12}$, then Disc1 operational mode occurred. Similarly to continuous mode in the first step the t_{1disc1} and and t_{2disc1} switching times should be calculated.

Without demonstration the switching times can be calculated as follows:

$$t_{1disc1} = \frac{3\sqrt{2}}{3U_{gb}U_{dc} + U_{dc}^2}H \text{, where}$$

$$H = \sqrt{T_c L i_{bdisc1ref} U_{gb} U_{dc}(3U_{gb} + U_{dc})} . \tag{21}$$

$$t_{2disc1} = -T_c \frac{U_{gb} + 2U_{gc}}{U_{dc}} \tag{22}$$

The current conduction time of the diode is:

$$t_{ddisc1} = \frac{\sqrt{2}(3U_{gb} + U_{dc})}{U_{gb}(3U_{gb}U_{dc} + U_{dc}^2)}H . \tag{23}$$

In the next step similarly to continuous mode the average value of phase *c* current is calculated. Without demonstration the average value is:

$$i_{cdisc1AV} = -\frac{1}{4T_c L}(t_{2disc1}U_{dc} + T_c^2 U_{gb} + I) \text{, where}$$

$$I = 2T_c^2 U_{gc} - 2T_c t_{ddisc1} U_{gb} + t_{ddisc1}^2 U_{gb} + J$$

$$J = -t_{2disc1}^2 U_{gb} - t_{1disc1}(T_c U_{gb} + 2T_c U_{gc}) + K$$

$$K = -t_{2disc1}^2 U_{gc} + t_{1disc1}t_{2disc1}U_{gb} + L$$

$$L = t_{2disc1}t_{1disc1}(U_{gc} + U_{ga} - U_{dc}) + M$$

$$M = -t_{1disc1}t_{ddisc1}U_{gb} - t_{2disc1}^2 U_{ga} . \tag{24}$$

If $i_{bavref} > i_{bdisc12}$, then *Disc2* operational mode occurred. Similarly to *Disc1* mode in the first step the t_{1disc2} and t_{2disc2} switching times should be calculated. Without demonstrations the switching times can be calculated as follows:

$$t_{1disc2} = \frac{T_c}{(9U_{gb}^2 - 4U_{dc}^2)U_{dc}}(4U_{dc}^2 U_{gc} + O) \text{, where}$$

$$O = 2U_{dc}^2 U_{gb} + 6U_{gb}U_{gc}U_{dc} + 3U_{dc}U_{gb}^2 + \sqrt{3P}$$

$$P = T_c^2 U_{gb}(2U_{dc} + 3U_{gb})(9U_{gb}^4 + 36U_{gb}^2 U_{gc} + Q)$$

$$Q = 3U_{dc}U_{gb}^3 + 12U_{dc}U_{gc}U_{gb}^2 - 4U_{dc}^2 U_{gb}^2 + R$$

$$R = 36U_{gc}^2 U_{gb}^2 - 16U_{dc}^2 U_{gc}U_{gb} + S$$

$$S = -18U_{gb}i_{bdisc2ref}L\frac{U_{dc}^2}{T_c} + T$$

$$T = -16U_{dc}^2 U_{gc}^2 + 12U_{dc}^3 i_{bdisc2ref}\frac{L}{T_c} . \tag{25}$$

Furthermore:

$$t_{2disc2} = -T_c \frac{U_{gb} + 2U_{gc}}{U_{dc}} \tag{26}$$

$$t_{ddisc2} = -T_c \frac{6U_{dc}(U_{gb}^2 + 12U_{gb}U_{gc}) + \sqrt{3P}}{3U_{gb}U_{dc}(3U_{gb} - 2U_{dc})} . \tag{27}$$

Similarly to *Disc1* calculating the average value of the phase *c* current, without demonstration:

$$i_{cdisc2AV} = \frac{-1}{12T_c L}(U_{gb}(3t_{ddisc2}^2 + 3T_c^2) + U) \text{, where}$$

$$U = 6T_c^2 U_{gc} - 6T_c t_{ddisc2}U_{gb} - 3t_{2disc2}T_c U_{gb} + V$$

$$V = -3t_{1disc2}^2 U_{gb} - 2t_{1disc2}^2 U_{dc} + 2t_{1disc2}t_{2disc2}U_{dc} + W$$

$$W = -6t_{2disc2}T_c U_{gc} + 3t_{2disc2}t_{ddisc2}U_{gb} + X$$

$$X = 3t_{1disc2}t_{2disc2}U_{gb} . \tag{28}$$

The third operational mode is the *Disc3*, which occurs if the load is very small and the voltage of the phase *b* is near to zero. Similarly to the previous operational modes without demonstration the switching times are:

$$t_{1disc3} = \frac{-T_c}{2u_{dc}(3u_{gb} + u_{dc})}\left(3u_{gb}^2 + 4u_{dc}u_{gb} + Y\right)$$
, where

$$Y = 6u_{gc}u_{gb} + u_{dc}^2 + 2u_{dc}u_{gc} + Z$$

$$Z = \sqrt{-T_c(9u_{gb}^2 - u_{dc}^2)(T_c\alpha)}$$

$$\alpha = u_{gb}^2 + 2u_{dc}u_{gb} + 4u_{gc}u_{gb} + 4u_{dc}u_{gc} + \beta$$

$$\beta = 4u_{gc}^2 + u_{dc}^2 + \frac{12i_{bdiscref}L_{13}u_{dc}}{T_c}$$
.
(29)

Furthermore:

$$t_{2disc3} = -T_c\frac{u_{gb} + 2u_{gc}}{u_{dc}}$$

For the current controller calculating the average value of the phase c without demonstration:

$$i_{cdisc3AV} = -\frac{u_{dc}^2(\chi) + \delta}{12T_cL_{13}(3u_{gb} - u_{dc})}$$
, where

$$\chi = t_{1disc3}t_{2disc3} - 3t_{2disc3}^2 + 2t_{1disc3}^2$$

$$\delta = u_{dc}T_c(9u_{gb}t_{1disc3} - 6u_{gb}t_{2disc3} + \varepsilon) + u_{dc}\phi$$

$$\varepsilon = u_{dc}T_c(6u_{gc}t_{1disc3} - 6u_{gc}T_c)$$

$$\phi = -15u_{gb}t_{1disc3}t_{2disc3} + 12u_{gb}t_{2disc3}^2 + \varphi$$

$$\varphi = 6u_{gb}t_{1disc3}^2 + T_c(9u_{gb}^2T_c + 9u_{gb}^2t_{1disc3}) + \gamma$$

$$\gamma = T_c(-18u_{gb}u_{gc}t_{1disc3} + 18u_{gb}u_{gc}T_c)$$
.
(30)

V. THE CONTROL METHOD

The structure for the current controller for continuous current mode can be seen at Fig. 8.

The reference for the average phase currents (i_{bAVref} and i_{cAVref}) come from the DC voltage controller. According to (11) and (12) the difference between the sampled and average values is estimated. Adding the average reference the result is the reference for the sampled value (i_{b0ref}, i_{c0ref}). We used proportional control for the current loop.

For the control needed yet the decoupling matrix **P** against the cross-coupling of the phases. The matrix contains two equations, which descript the contact between the change of the current of the other phase and the change of the voltage of the current phase. The results of the equations are the follows:

$$\Delta t_1 = -L\frac{di_c + 2di_b}{u_{dc}}$$
(31)

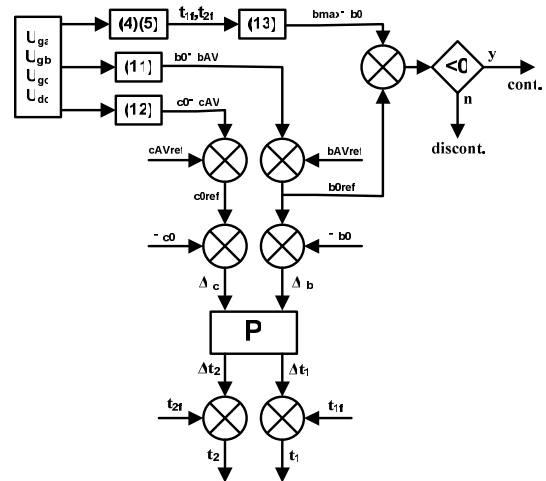$$\Delta t_2 = -L\frac{di_b + 2di_c}{u_{dc}}$$
.
(32)

Fig. 8 Current controller for continuous current mode

The control structure was the same for discontinuous current mode as well, but the equations were substituted with the corresponding ones.

VI. CONCLUSION

With the new developed 3SC control we could make a high efficiency and reliable PV converter, which satisfy the prescriptions and limitations of the standards. The 3SC controls were verified with some simulation, and it is work correctly in the whole load range.

REFERENCES

[1] A. Balogh, Z. Bilau, I. Varjasi, S. Halasz, "High Efficiency Control of a Grid Connected PV Converter", In Proc. of EuroPES2007, Palma de Mallorca, Spain.
[2] I. Varjasi, A. Balogh, S. Halasz, "Sensorless Control of a Grid Connected PV Converter", in Proc. PEMC2006, Portoroz, Slovenia.
[3] IEC 61727 International Standard, Photovoltaic (PV) systems - Characteristics of the utility interface, Switzerland, 2004.
[4] A. Balogh, I. Varjasi, Discontinuous Current Mode of a Grid Connected PV Converter, IYCE2007, Budapest, Hungary
[5] I. Varjasi, A. Balogh, S. Halasz, Sensorless control of a grid connected PV converter, EPE-PEMC2006, Portoroz., Slovenia.
[6] A. Balogh, Z.T. Bilau and I. Varjasi, High Efficiency Control of a Grid Connected PV Converter. In Proc. of EuroPES2007, Palma de Mallorca, Spain.
[7] Attila Balogh, Zoltán Tamás Bilau, Istvan Varjasi Control Algorithm for High Efficiency Grid Connected PV Converters. In Proc. of IWCIT 2007, Ostrava, Czech Republic.
[8] Attila Balogh, Eszter Varga, István Varjasi: 3SC for Grid Connected Converters, In Proc. of Power and Energy Systems Conference (EuroPES 2008), Corfu, Greece, 2008.
[9] Attila Balogh, Zoltan Tamás Bilau, István Varjasi, Sándor Halász: High Efficiency Control of a Low Noise PV Converter, In Proc. of Mezsdunarodnaja Naucsno-Tehnicseszkaja Konferencija,Tomszk, Russia, 2007.

Attila Balogh was born on March 5 1982 in Pápa, received the Electrical Engineering degree from the Budapest University of Technology and Economics, Budapest, Hungary, in 2006. Since 2006, he has been a Ph.D. student in the Department of Automation and Applied Informatics at the Budapest University of Technology and Economics (BUT). His research field involves control strategies, FPGA based process control, servo drives and renewable energy.

He has attended international conferences several times and has worked in some research projects, as well.

Mr. Balogh is member of Hungarian Electrotechnical Association.

Eszter Varga was born on November 21 1983 in Szekszárd, she is an Architect student at the Budapest University of Technology and Economics (BUT). Her research field involves application of renewable energy sources, buildings-constructions for solar technology and efficiency increasing methods for PV cells.

She has attended international conferences several times and has worked in some research projects, as well.

Ms. Varga is member of ESN.

István Varjasi was born on September 20 1956 in Soltvadkert, received the Electrical Engineering and Ph.D. degrees from the Budapest University of Technology and Economics, Budapest, Hungary, in 1980 and 1997. Since 1998, he has been an Associate Professor in the Department of Automation and Applied Informatics at the Budapest University of Technology and Economics (BUT). His research field involves control strategies, FPGA based process control, servo drives and renewable energy.

He has attended international conferences several times and has worked in some research projects, as well.

Dr. Varjasi is member of Hungarian Electrotechnical Association.